CMS Physics Analysis Summary

Contact: cms-pag-conveners-susy@cern.ch 2015/12/15

Search for SUSY in same-sign dilepton events at $\sqrt{s} = 13$ TeV

The CMS Collaboration

Abstract

A search for new physics is performed using events with a pair of isolated same-sign leptons and jets in the final state using the CMS detector. Results are based on a sample of proton-proton collisions at a centre-of-mass energy of 13 TeV at the LHC corresponding to an integrated luminosity of 2.2 fb^{-1}. In order to be sensitive to a wide variety of possible signals beyond the standard model, we consider multiple search regions defined by the missing transverse energy, the hadronic transverse energy, the transverse mass, the number of jets and b quark jets, and the transverse momenta of the leptons in the event. No excess above the standard model background expectation is observed and constraints are set on the gluino pair production cross section; model independent limits and selection efficiencies are also provided for additional model testing.

1 Introduction

The search for new physics in the same-sign (SS) dilepton final state is greatly motivated by the limited number and low cross section of the standard model processes yielding such a signature and by various new physics processes resulting in this final state. Examples include supersymmetric (SUSY) particles, Majorana neutrinos, vector-like quarks, and SS top quark pair production. Within the SUSY framework the main focus of this signature is on gluino pair production that could lead to SS dilepton production due to the Majorana nature of gluino, which allows gluino pairs to decay via SS charginos, yielding two W bosons of the same sign. Gluino pair production could also yield four top quarks in the decay chain, which may result in the SS dielpton final state. Alternatively, cascade decays of pair produced squarks could also lead to the same signature.

Searches for SS dileptons have been carried out previously by the CMS experiment [1] at the CERN LHC, and the results have been published for different analysis strategies [2, 3]. The analysis based on a $\sqrt{s} = 8$ TeV dataset corresponding to an integrated luminosity of 19.5 fb^{-1} [3] probed gluino masses in the four top quark signature up to about 1050 GeV.

This note describes a new physics search with SS dileptons based on 13 TeV data collected with the CMS detector in 2015. The strategy of the search resembles the latest 8 TeV result [3], but the kinematic regions are redefined to accommodate higher mass range reachable with new energy frontier. At the same time, improvements in the event selection and background estimation techniques increase the analysis universality and its sensitivity to new physics scenarios.

2 Event selection and Monte Carlo simulation

Events for the analysis are selected with two sets of online algorithms. The first one combines a set of dilepton high-level triggers (HLT) that require two very loosely isolated leptons with $p_{\text{T}} > 17\,\text{GeV}$ for the leading lepton, and $p_{\text{T}} > 8$ (12) GeV for the trailing muon (electron). The second set of triggers selects events with a lowered p_{T} threshold for two leptons ($p_{\text{T}} > 8\,\text{GeV}$) and without any restriction on their isolation, but in addition requires hadronic activity of $H_{\text{T}}^{\text{HLT}} > 300\,\text{GeV}$ in the event, where $H_{\text{T}}^{\text{HLT}}$ is the scalar sum of p_{T} of all jets with $p_{\text{T}} > 40\,\text{GeV}$ and $|\eta| < 3.0$ identified at the HLT. Typical trigger efficiencies on the plateau are 94% (98%) per muon (electron) legs and 100% for H_{T}.

In the offline selection, at least two well-identified and isolated SS leptons (ee, eμ, or $\mu\mu$) with invariant mass greater than 8 GeV and at least two jets are required.

Muon candidates are reconstructed combining the information from both the silicon tracker and the muon spectrometer in a global fit [4]. An identification selection is performed using the quality of the geometrical matching between the tracker and the muon system measurements. The quality of the muon charge reconstruction is ensured by an additional criterion on the track quality: $\delta p_{\text{T}}(\mu)/p_{\text{T}}(\mu) < 0.2$.

Electron candidates are reconstructed combining clusters of energy deposits in the electromagnetic calorimeter and tracks in the silicon tracker [5]. An identification selection is performed using a multivariate discriminant built with shower shape and track quality variables. The nominal selection criteria are designed to have maximum rejection of electron candidates from QCD multijet production while maintaining approximately 90% efficiency for electrons from the decay of W/Z bosons; a relaxed selection on the multivariate discriminant is used for the "loose" definition of electron identification. The quality of the electron charge reconstruction is ensured by requiring consistency between the independent measurements of the charge from

the ECAL energy deposit and the inner tracker. To suppress electrons arising from photon conversions, those with missing hits in the innermost layers of the tracking system are rejected.

Both lepton candidates in the event must be consistent with originating from the same collision vertex. Their transverse impact parameter should not exceed 0.5 mm, longitudinal impact parameter should be less than 1 mm, and the 3D impact parameter significance should be smaller than 4.

The charged leptons produced in decays of heavy particles, such as W and Z bosons or SUSY particles, are typically spatially isolated from the hadronic activity in the event, while the leptons produced in the decays of hadrons or misidentified leptons are usually embedded in jets. This distinction becomes less evident moving to highly boosted systems where decay products tend to overlap. Therefore, given the higher collision energy explored in this analysis, a new and improved isolation definition is constructed using three variables as input:

- A mini-isolation (I_{mini}) [6] which is computed as a ratio of the scalar sum of transverse momenta of the charged hadrons, neutral hadrons, and photons within a cone of radius $R(p_{\text{T}}^{\ell})$ around the lepton candidate direction at the origin, to the transverse momentum of the candidate. The cone radius R depends on lepton p_{T} as

$$R(p_{\text{T}}^{\ell}) = \frac{10\,\text{GeV}}{\min\left[\max\left(p_{\text{T}}^{\ell}, 50\,\text{GeV}\right), 200\,\text{GeV}\right]}. \tag{1}$$

  The varying isolation cone definition takes into account the aperture of b hadron decays as a function of their p_{T}, and reduces the inefficiency from accidental overlap between the lepton and jets in a busy event environment.

- A ratio between the lepton p_{T}^{ℓ} and $p_{\text{T}}^{\text{jet}}$ of a jet containing the lepton:

$$p_{\text{T}}^{\text{ratio}} = \frac{p_{\text{T}}^{\ell}}{p_{\text{T}}^{\text{jet}}}. \tag{2}$$

  The $p_{\text{T}}^{\text{ratio}}$ variable acts as a relative isolation in a larger cone. It improves mini-isolation performance when there are no nearby jets, expecially for low-p_{T} leptons.

- Transverse momentum of the lepton relative to the residual momentum of the closest jet after lepton momentum subtraction:

$$p_{\text{T}}^{\text{rel}} = \frac{(\vec{p}(\text{jet}) - \vec{p}(\ell)) \cdot \vec{p}(\ell)}{|\vec{p}(\text{jet}) - \vec{p}(\ell)|}. \tag{3}$$

  The $p_{\text{T}}^{\text{rel}}$ variable allows to identify leptons that accidentally overlap with other jets in the event.

A lepton is considered to be isolated if the following condition is respected:

$$I_{\text{mini}} < I_1 \wedge (p_{\text{T}}^{\text{ratio}} > I_2 \vee p_{\text{T}}^{\text{rel}} > I_3) \tag{4}$$

The values of $I_{\text{i}}, i = 1, 2, 3$, depend on the lepton flavor; as the probability to misidentify a lepton is higher for electrons, tighter isolation values are used in this case (see Table 1).

A lepton passing the full set of selection criteria is not considered if it forms an opposite-sign same-flavor pair with another loosely identified lepton in the event such that their invariant mass ($m_{\ell\ell}$) satisfies $m_{\ell\ell} < 12\,\text{GeV}$ or $76 < m_{\ell\ell} < 106\,\text{GeV}$. These requirements are introduced

Table 1: Multi-isolation working points used in the analysis.

Isolation value	Loose leptons	Tight muons	Tight electrons
I_1	0.4	0.16	0.12
I_2	0	0.76	0.80
I_3(GeV)	0	7.2	7.2

to reduce backgrounds from processes with low-mass bound states, $\gamma^* \to \ell^+\ell^-$, and processes with Z boson production.

Jets and $E_{\mathrm{T}}^{\mathrm{miss}}$ are reconstructed with the particle-flow algorithm [7]. For jet clustering, the anti-k_{T} algorithm with a distance parameter of 0.4 [8] is utilized. Jets are required to pass quality requirements [9] to remove those consistent with calorimeter noise. After the expected contribution from extra pp collisions is subtracted, jet energies are corrected for residual non-uniformity and nonlinearity of the detector response using corrections found with collision data [9]. Jets are required to have $p_{\mathrm{T}} > 40\,\mathrm{GeV}$, be within the tracker acceptance $|\eta| < 2.4$, and be separated from loosely identified leptons by a distance of $\Delta R > 0.4$. Hadronic activity in the event is defined as the scalar sum of selected jet p_{T}'s: $H_{\mathrm{T}} = \sum_{\mathrm{jets}} p_{\mathrm{T}}$.

To identify jets originating from b quarks, a combined secondary vertex algorithm is used. Jets with $p_{\mathrm{T}} > 25\,\mathrm{GeV}$ and $|\eta| < 2.4$ are considered as b-tagged if they pass the medium working point of the algorithm, which provides around 70% efficiency with a mistag rate less than 1% [10, 11].

Kinematic selections for leptons, jets, and b-tagged jets are listed in Table 2.

Table 2: Kinematic and fiducial requirements on tight (loose) leptons and jets that are used in the analysis.

Object	p_{T} (GeV)	$\lvert\eta\rvert$
Electrons	>15 (7)	<2.5
Muons	>10 (5)	<2.4
Jets	>40	<2.4
b-tagged jets	>25	<2.4

Monte Carlo (MC) simulations, which include pileup effects from additional pp collisions, are used to estimate the SM background processes with two prompt leptons of the same sign (see Section 4) and to calculate the efficiency for various new physics scenarios. The SM background samples are generally produced with the MADGRAPH5_AMC@NLO program [12] at leading order (LO) or next-to-leading order (NLO) in perturbative QCD, with the exception of diboson samples which are generated using POWHEG [13]. The PYTHIA 8 generator [14] is used to simulate parton showering and hadronization. The CMS detector response is modeled with the GEANT4 package [15].

The SUSY signal samples are generated with MADGRAPH5_AMC@NLO program [12] at LO precision, allowing up to two additional partons to be present in the matrix element calculations. Parton showering and hadronization, as well as decays of SUSY particles are simulated with PYTHIA 8. The detector simulation is carried out with the CMS fast simulation package [16]. A series of cross checks is performed to ensure that fast simulation results are in agreement with the ones obtained with GEANT4-based detector simulation. Simulated events are processed with the same chain of reconstruction programs that is used for data.

3 Search strategy

Signal models that can lead to the experimental signature of SS lepton pairs mainly differ in the numbers of W bosons, b jets, and light-flavor jets produced in decays of SUSY particles. In addition, for each model, the mass difference between the SUSY particles involved in the decay chain leads to either energetic or soft decay products, implying differences in the event kinematic variables such as the p_T of the leptons, the H_T, and the E_T^{miss}.

For instance, strongly produced R-parity-conserving simplified SUSY models can feature four W bosons and four b jets, or four W bosons and two b jets, or two W bosons and four light-flavor jets.

Models in the first category can be obtained through gluino pair production resulting in the $t\bar{t}t\bar{t}\widetilde{\chi}_1^0\widetilde{\chi}_1^0$ final state, where $\widetilde{\chi}_1^0$ is the lightest neutralino (LSP). If the gluino is lighter than squarks of the first two generations, and the top squark is the lightest squark, the gluino ungergoes a three-body decay $\widetilde{g} \to t\bar{t}\widetilde{\chi}_1^0$ mediated by an off-shell top squark (T1tttt model in Fig. 1a). If the top squark is light enough to be on-shell, the gluinos decay as $\widetilde{g} \to \widetilde{t}\bar{\widetilde{t}} \to t\bar{t}\widetilde{\chi}_1^0$ (T5tttt model in Fig. 1b). Events in the first category are typically characterized by large H_T, E_T^{miss}, N_{jets}, and $N_{b\,jets}$, but this is not necessarily true in the compressed regions of the mass spectrum where soft decay products (leptons, b jets, light-flavor jets) are mostly present in the final state. In particular, when the mass difference between the top squark and the LSP is very small (about 20 GeV) we are basically blind to the b jets arising from the top squark decay, and the two off-shell W bosons, if decaying leptonically, yield very soft leptons. In this case, large E_T^{miss} is accompanied by intermediate H_T and lower number of jets in comparison to less compressed regions of the parameter space. The same experimental signature can be obtained with the gluinos undergoing a three-body decay $\widetilde{g} \to \bar{t}b\widetilde{\chi}^{\pm}$, under the assumption that the bottom squark ($\widetilde{b}$) is the lightest squark, still too heavy to be on-shell (T5ttbbWW model in Fig. 1c).

Signatures with four W and two b jets in the final state can result from bottom squark pair production, where each bottom squark decays to a top quark and a chargino, and the chargino decays into an LSP and a (possibly off-shell) W boson (T6ttWW model in Fig. 1d).

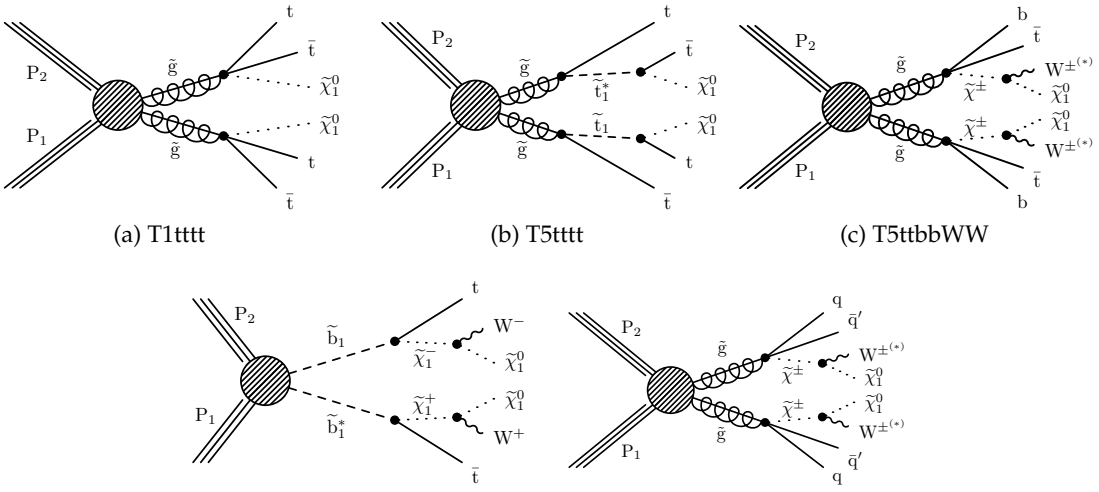

Figure 1: Diagrams for possible SUSY processes yielding two same-sign leptons in the final state.

Finally SS lepton pairs can be produced in association with large H_T, E_T^{miss}, and N_{jets} but without b jets. In particular, final states with two W bosons and four light-flavor jets can result

from gluino pair production, where each gluino decays into two light quarks and a chargino. Charginos of the two chains each decay into a W boson and a LSP and can have the same charge (T5qqqqWW model in Fig. 1e); in case the difference in mass between the chargino and the LSP is small, the W bosons are off-shell and produce soft leptons.

Therefore, in order to be sensitive to a wide range of SUSY topologies, different variables are used to define signal regions. The chosen division is also motivated by the properties of the SM processes, and it leads to different composition of the background in these regions, increasing the sensitivity of the search.

First of all three exclusive lepton selections are defined:

- high-high (HH) selection : two tight leptons with $p_{\mathrm{T}} > 25\,\mathrm{GeV}$,
- high-low (HL) selection : one tight lepton with $10 < p_{\mathrm{T}} < 25\,\mathrm{GeV}$ and one tight lepton with $p_{\mathrm{T}} > 25$ GeV,
- low-low (LL) selection : two tight leptons with $10 < p_{\mathrm{T}} < 25\,\mathrm{GeV}$.

The HH selection is designed to search for signals producing high-p_{T} leptons, while the HL and LL selections are more sensitive to signals producing soft leptons. In different signal models all or some of the W bosons produced in the signal decay chain can be off-shell in compressed scenarios, leading to one or two soft leptons. Moreover, the high lepton p_{T} threshold suppresses the contribution from nonprompt leptons, so the HH region is mainly populated by irreducible SM backgrounds. The nonprompt lepton background is largely contained in the HL region, where typically the high-p_{T} lepton is prompt and the low-p_{T} one is nonprompt. The LL region is characterized by very small background, since all processes where at least one lepton originates from an on-shell vector boson are suppressed by the low-p_{T} requirement.

Signal regions are then defined separately for HH, HL, and LL selections. The general approach is similar to the one used in 8 TeV analysis [3]: the search regions are formed using H_{T}, $E_{\mathrm{T}}^{\mathrm{miss}}$, N_{jets}, and $N_{\mathrm{b\,jets}}$ variables; N_{jets} and $N_{\mathrm{b\,jets}}$ separate backgrounds and signal models with different jet and b jet multiplicities, while bins in H_{T} and $E_{\mathrm{T}}^{\mathrm{miss}}$ increase the sensitivity to different points in the SUSY mass spectrum.

In addition, a new kinematic variable $M_{\mathrm{T}}^{\mathrm{min}}$ is introduced:

$$M_{\mathrm{T}}^{\mathrm{min}} = \min\left(M_{\mathrm{T}}(\ell_1, E_{\mathrm{T}}^{\mathrm{miss}}), M_{\mathrm{T}}(\ell_2, E_{\mathrm{T}}^{\mathrm{miss}})\right).$$

In case of a SS lepton pair in the $\mathrm{t\bar{t}}$ process, this variable has a cutoff at the W boson mass. Therefore, forming search regions with an upper boundary on $M_{\mathrm{T}}^{\mathrm{min}}$ of 120 GeV allows to contain nonprompt background in dedicated search regions where finer kinematic binning allows to discriminate against the $\mathrm{t\bar{t}}$ process. Consequently, search regions with $M_{\mathrm{T}}^{\mathrm{min}} > 120\,\mathrm{GeV}$ profit from reduced $\mathrm{t\bar{t}}$ background.

The summary of the selection is described in Tables 3–5. All signal regions are exclusive and are further combined statistically to yield the final results (Section 6).

4 Backgrounds

Backgrounds for the SS dilepton final state can be divided in three categories:

- **Nonprompt leptons:** Nonprompt leptons are leptons from heavy-flavor decays, misidentified hadrons, muons from light-meson decays in flight, or electrons from unidentified photon conversions. Depending on the signal regions, this background

Table 3: Signal region definitions for the HH lepton selection.

$N_{\text{b jets}}$	$M_{\text{T}}^{\text{min}}$ (GeV)	$E_{\text{T}}^{\text{miss}}$ (GeV)	N_{jets}	$H_{\text{T}} < 300\,\text{GeV}$	$H_{\text{T}} \in [300, 1125]\,\text{GeV}$	$H_{\text{T}} > 1125\,\text{GeV}$
0	< 120	$50 - 200$	2-4	SR1	SR2	SR32
			5+	SR3	SR4	
		$200 - 300$	2-4		SR5	
			5+		SR6	
	> 120	$50 - 200$	2-4		SR7	
			5+		SR8	
		$200 - 300$	2-4			
			5+			
1	< 120	$50 - 200$	2-4	SR9	SR10	
			5+	SR11	SR12	
		$200 - 300$	2-4		SR13	
			5+		SR14	
	> 120	$50 - 200$	2-4		SR15	
			5+		SR16	
		$200 - 300$	2-4			
			5+			
2	< 120	$50 - 200$	2-4	SR17	SR18	
			5+	SR19	SR20	
		$200 - 300$	2-4		SR21	
			5+		SR22	
	> 120	$50 - 200$	2-4		SR23	
			5+		SR24	
		$200 - 300$	2-4			
			5+			
3+	< 120	$50 - 200$	2+	SR25	SR26	
		$200 - 300$	2+	SR27	SR28	
	> 120	> 50	2+	SR29	SR30	
inclusive	inclusive	> 300	2+		SR31	

is dominated by $\mathrm{t\bar{t}}$ and W + jets processes; it represents the largest backgrounds for regions with low $M_{\text{T}}^{\text{min}}$ and low H_{T}.

- **SM processes with SS leptons:** Standard model processes yield SS leptons, mostly from diboson production and bosons produced in association with a pair of top quarks; the dominant sources are WZ and $\mathrm{t\bar{t}W}$ events for signal regions with zero and one or more b jets, respectively. They are the largest background in the signal regions defined by very tight selection requirements.
- **Charge misidentification:** Events with opposite-sign isolated leptons where the charge of one electron is misidentified because of severe bremsstrahlung in the tracker material. Overall, this is a small background.

Nonprompt lepton background is estimated from data using the "tight-to-loose" (TL) ratio method, which was already employed in previous versions of the analysis, but has been revisited and improved. It is based on a control sample of events (application region) where one lepton fails the nominal selection but passes looser requirements defined by relaxing the isolation selection for muons and both isolation and identification for electrons. Events in this control region are reweighted by $\text{TL}/(1 - \text{TL})$, where TL is the probability for a nonprompt lepton passing the loose selection to also pass the tight selection. This probability is measured in a QCD-enriched data set (measurement region), from single-lepton events after a selection

Table 4: Signal region definitions for the HL lepton selection.

$N_{\text{b jets}}$	$M_{\text{T}}^{\text{min}}$ (GeV)	$E_{\text{T}}^{\text{miss}}$ (GeV)	N_{jets}	$H_{\text{T}} < 300\,\text{GeV}$	$H_{\text{T}} \in [300, 1125]\,\text{GeV}$	$H_{\text{T}} > 1125\,\text{GeV}$
0	< 120	$50 - 200$	2-4	SR1	SR2	SR26
			5+	SR3	SR4	
		$200 - 300$	2-4		SR5	
			5+		SR6	
1	< 120	$50 - 200$	2-4	SR7	SR8	
			5+	SR9	SR10	
		$200 - 300$	2-4		SR11	
			5+		SR12	
2	< 120	$50 - 200$	2-4	SR13	SR14	
			5+	SR15	SR16	
		$200 - 300$	2-4		SR17	
			5+		SR18	
3+	< 120	$50 - 200$	2+	SR19	SR20	
		$200 - 300$	2+	SR21	SR22	
inclusive	> 120	$50 - 300$	2+	SR23	SR24	
inclusive	inclusive	> 300	2+		SR25	

Table 5: Signal region definitions for the LL lepton selection. The $H_{\text{T}} > 300\,\text{GeV}$ requirement is applied in all search regions in this category.

$N_{\text{b jets}}$	$M_{\text{T}}^{\text{min}}$ (GeV)	H_{T} (GeV)	$E_{\text{T}}^{\text{miss}} \in [50 - 200]\,\text{GeV}$	$E_{\text{T}}^{\text{miss}} > 200\,\text{GeV}$
0	< 120	> 300	SR1	SR2
1	< 120		SR3	SR4
2	< 120		SR5	SR6
3+	< 120		SR7	
inclusive	> 120		SR8	

suppressing electroweak processes (Drell–Yan and W + jets) and after subtracting their residual contribution. The measurement is done as function of the lepton p_{T} and η, separately for each lepton flavor (e or μ) and trigger (with or without isolation).

The method works as long as the probability measured in the measurement region is the same as in the application region; any discrepancy will lead to an incorrect prediction. The main sources of discrepancies are identified as differences in the momentum spectrum and the flavor of the parton producing the nonprompt lepton. These two effects are mitigated in the following way. The TL ratio is parameterized as a function of $p_{\text{T}}^{\text{corr}}$, defined as the lepton p_{T} plus the energy in the isolation cone exceeding the isolation threshold value — this quantity is highly correlated with the mother parton p_{T}, and thus the parameterization is more robust against mother parton p_{T} variations. The second effect, i.e. flavor dependence, is relevant for electrons only; in fact nonpompt muons originate predominantly from heavy-flavor decays, while in the case of electrons there are also sizable contributions from light-flavor quarks and conversions. The effect of variations in the flavor composition is suppressed by adjusting the loose electron identification criteria so that the numerical value of the TL ratio for electrons from light flavors matches the one for electrons from heavy flavors. The procedure to define the loose electron working point is carried out in a $\text{t}\bar{\text{t}}$ MC sample, and the result is validated in data by verifying that no significant variation in the TL ratio measurement is observed in the presence or absence of b jets in the event.

As a cross-check of the prediction, along the lines of what was done in a recent ATLAS pub-

lication [17], an alternative TL ratio measurement is performed in the dilepton control region where one of the leptons fails the impact parameter requirement; the predictions from the two methods are found to be consistent, both in MC samples and in data.

Standard model processes with prompt SS leptons are, with the exception of WZ production, estimated from simulation accounting for both theoretical and experimental uncertainties. The WZ background is normalized to data in a control region defined requiring at least two jets, no b jets, $E_{\mathrm{T}}^{\mathrm{miss}} > 30\,\mathrm{GeV}$, and three leptons, where two of them form a same-flavor, opposite-sign pair with the invariant mass within 15 GeV of the Z boson mass. After correcting for the normalization, we rely on the simulated sample to predict the yield of background events in the signal regions. The measured normalization factor is found to be compatible with unity at a 1σ level.

The charge misidentification background is estimated by reweighting events with opposite-sign lepton pairs by the charge misidentification probability. For electrons, this probability is extracted from simulation and is in the range $\mathrm{O}(10^{-5})$–$\mathrm{O}(10^{-3})$ depending on the electron p_{T} and η. The prediction is validated using the $\mathrm{Z} \to \mathrm{e}^{\pm}\mathrm{e}^{\pm}$ mass peak and is found to underestimate the observed yield by about 35%; after correcting for the observed discrepancy, we find good agreement with the prediction for all kinematic variables used in the analysis. The charge misidentification probability is negligible for muons [18].

5 Systematic uncertainties

The different sources of systematic uncertainties are presented in this section; the overall effects on each process normalization and shape are summarized in Table 6.

Experimental sources of uncertainty are mostly related to the corrections applied to the simulation to better describe the data. These uncertainties affect the expected signal and backgrounds yields estimated from simulation. The corrections applied to the jet energy scale (JES) in simulation have associated uncertainties, which vary the JES by 2–8%, depending of the transverse momentum and pseudorapidity of the jet. The impact of these uncertainties is assessed by shifting the jet energy correction factors for each jet up and down by 1σ before the calculation of all kinematic quantities. The variations are correlated among different signal regions as the overall bin-by-bin migration is allowed. Asymmetric variations of the JES are considered, leading to yield fluctuations of 2–10% for most of the signal regions and processes. A similar approach is used for the uncertainties associated with the corrections for the b tagging efficiencies for light-flavor and b quark jets, which are parametrized as a function of p_{T} and η. Considering only highly populated signal regions, typical variations due to b tagging are of the order of 5% for $\mathrm{t\bar{t}W}$. Lepton identification and trigger scale factors are computed with the "tag-and-probe" technique [4, 5] and are applied to the simulated samples to match the performance observed in data. An uncertainty of 2% is assigned to the lepton selection efficiency, and 4% is assigned to the trigger efficiency. Additional uncertainties are applied for signal samples simulated with the fast detector simulation. The simulated samples are reweighted to match the observed multiplicity of the number of collisions per event in data; the uncertainty on the minimum bias cross section is propagated to the final yields with an effect at the level of 5% or less.

The background sources estimated from simulation are also subject to theoretical uncertainties related to the unknown higher- order effects and to the uncertainties in the knowledge of the parton distribution functions (PDF). The first ones are estimated conventionally by varying the renormalization and factorization scales up and down by a factor two. The effect on the

overall cross section is found to be 13% for $t\bar{t}W$ and 11% for $t\bar{t}Z$ for the NLO computation [19]. The cross sections of these processes have been measured by CMS in 8 TeV data [20]. The results are consistent with theory but have larger uncertainties. In addition to the overall normalization, systematic uncertainties of theoretical origin in the distribution of the events in the final discriminating variables are considered. In particular an uncorrelated uncertainty in the acceptance corresponding to different signal regions is included (a 3% effect is assigned to the low-H_T categories and an 8% is assigned to the high-H_T ones). The magnitude of the uncertainties related to the PDF is obtained conventionally using the replicas of the NNPDF 3.0 set. The overall uncertainty is around 4% for the $t\bar{t}W$ and $t\bar{t}Z$ samples. Theoretical uncertainties are also considered for the remaining minor backgrounds estimated from simulation: a similar procedure is used for the $W^{\pm}W^{\pm}$ process leading to an overall uncertainty of 30%, while a conservative 50% is assigned to the other rare processes.

The remaining sources of uncertainty are those related to the methods based on data that are used to estimate the nonprompt lepton, charge misidentification, and WZ backgrounds. An overall normalization uncertainty of 30% is assigned to the nonprompt lepton background prediction; this uncertainty accounts for the performance of the method on simulated data and for the different prediction from the two alternative procedures described in Section 4. An additional systematic uncertainty comes from the subtraction of the prompt lepton contamination in the QCD measurement region; the overall effect on the nonprompt lepton background yield is between 1 and 20%, depending of the signal region considered and is larger for high-p_T leptons. Finally, we account for the statistical uncertainty in the number of events observed in the application region; these uncertainties are dominant in only in regions where we expect a negligible contribution from this source of background. The prediction of the background from charge misidentification is assigned an overall systematic uncertainty of 26%, from the nonclosure of the method before applying scale factors to correct the charge misidentification probability in simulation with respect to the one measured in data. The estimation of the WZ background is assigned a 30% normalization uncertainty from the total uncertainty in the control region, combining a statistical component and a systematic uncertainty in the subtraction of the non-WZ processes in the control region. Using the same procedure as described above, uncertainties in the extrapolation from the control region to the signal region are assessed from the propagation of the uncertainty in the JES and in the b tagging efficiencies.

Table 6: Summary of the sources of uncertainties and their effect on the total yield in signal regions. Reported values are representative for the most relevant signal regions.

Source	Typical Effect (%)
Luminosity	4.6
Lepton selection	2
Trigger efficiency	4
Pileup	5
Jet energy scale	2-10
b tagging	5
Monte Carlo stat.	1-30
Scale variations	11-30
Parton distributions	4
Nonprompt leptons	30-36
Charge misidentification	26
WZ normalization	30

6 Results

Distributions for the five kinematic variables used to define the signal regions (H_T, E_T^{miss}, M_T^{min}, N_{jets}, $N_{b\,jets}$) after a preselection are shown in Fig. 2, where the full background prediction is compared to data. The preselection (baseline) requires a SS lepton pair passing nominal selection criteria; it is defined inclusively in lepton p_T, M_T^{min}, N_{jets}, and $N_{b\,jets}$, while it requires E_T^{miss} larger than 30 GeV or H_T larger than 500 GeV. Event yields in the signal regions after full selection are presented in Fig. 3 and in Table 7; no significant deviation from the prediction is observed (the largest local significances are 2.3σ in HL SR8 and 1.7σ in HH SR10).

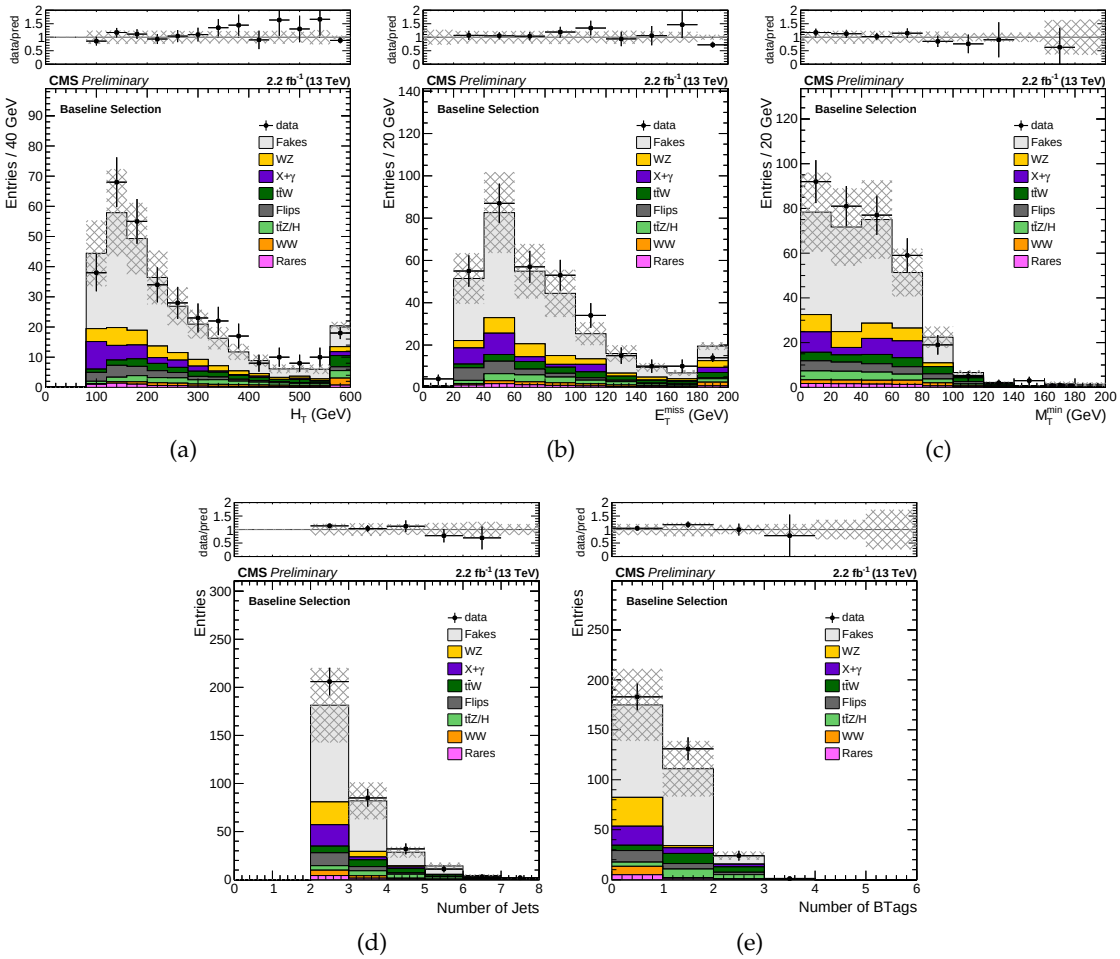

Figure 2: Distributions for the main analysis variables after the baseline selection with $\mathcal{L}$ = 2.2 fb^{-1}. The shaded area represents the total uncertainty in the background prediction.

Given the lack of a significant excess over the expected SM background, the results of the search are used to set limits on the gluino pair production in the T1tttt simplified model as a function of the mass of the gluino and the LSP. For each mass point in the SUSY particle mass spectrum, results from all signal regions are combined to extract exclusion limits at 95% confidence level (CL), using the LHC-type CL$_s$ method [21–23]. Log-normal nuisance parameters are used to account for the signal and background uncertainties which are described in Section 5 and summarized in Table 6. The resulting limits on the cross section times branching fraction, as well as the exclusion contours, are shown in Fig. 4. The exclusion contours are obtained with the gluino cross section claculated at NLO+NLL (next-to-leading logarithmic) accuracy, assuming that other SUSY particles are heavy enough to be decoupled [24–30].

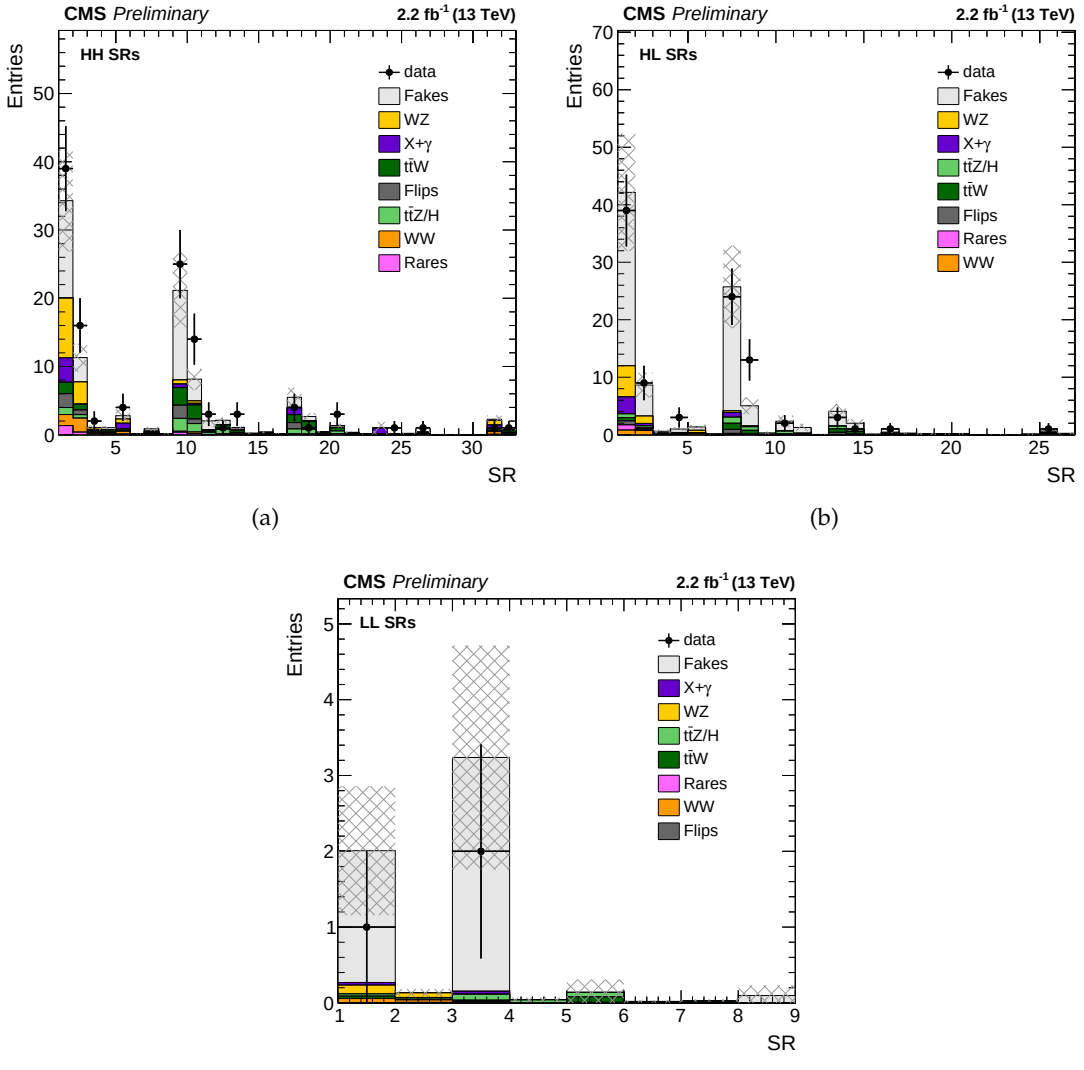

Figure 3: Event yields in HH (a), HL (b), and LL (c) signal regions with $\mathcal{L} = 2.2$ fb^{-1}. The shaded area represents the total uncertainty in the background prediction.

Table 7: Event yields in the signal regions with $\mathcal{L} = 2.2\ \text{fb}^{-1}$.

	HH regions		HL regions		LL regions	
	Expected SM	Observed data	Expected SM	Observed data	Expected SM	Observed data
SR1	34.4 ± 7.3	39	42.2 ± 10.9	39	2.01 ± 0.94	1
SR2	11.3 ± 1.8	16	8.7 ± 2.2	9	0.13 ± 0.05	0
SR3	1.01 ± 0.35	2	0.60 ± 0.34	0	3.2 ± 1.5	2
SR4	1.04 ± 0.23	0	0.99 ± 0.38	3	0.04 ± 0.03	0
SR5	2.8 ± 1.0	4	1.35 ± 0.37	0	0.14 ± 0.17	0
SR6	0.10 ± 0.05	0	0.08 ± 0.03	0	0.02 ± 0.01	0
SR7	0.87 ± 0.31	0	25.8 ± 7.6	24	0.03 ± 0.01	0
SR8	0.15 ± 0.10	0	5.1 ± 1.5	13	0.10 ± 0.10	0
SR9	21.2 ± 5.2	25	0.32 ± 0.20	0		
SR10	8.2 ± 1.4	14	2.36 ± 0.99	2		
SR11	2.04 ± 0.92	3	1.26 ± 0.65	0		
SR12	2.14 ± 0.39	1	0.05 ± 0.04	0		
SR13	1.06 ± 0.21	3	4.1 ± 1.3	3		
SR14	0.24 ± 0.11	0	2.01 ± 0.69	1		
SR15	0.35 ± 0.11	0	0.05 ± 0.03	0		
SR16	0.17 ± 0.07	0	0.42 ± 0.10	1		
SR17	5.5 ± 1.4	4	0.28 ± 0.15	0		
SR18	2.70 ± 0.46	1	0.09 ± 0.25	0		
SR19	0.43 ± 0.08	0	0.10 ± 0.09	0		
SR20	1.36 ± 0.24	3	0.15 ± 0.10	0		
SR21	0.36 ± 0.10	0	0.002 ± 0.001	0		
SR22	0.08 ± 0.04	0	0.03 ± 0.04	0		
SR23	0.98 ± 0.93	0	0.03 ± 0.02	0		
SR24	0.13 ± 0.04	1	0.05 ± 0.09	0		
SR25	0.18 ± 0.06	0	0.81 ± 0.25	1		
SR26	0.42 ± 0.11	1	0.24 ± 0.12	0		
SR27	0.004 ± 0.015	0				
SR28	0.03 ± 0.02	0				
SR29	0.014 ± 0.008	0				
SR30	0.02 ± 0.01	0				
SR31	2.28 ± 0.61	1				
SR32	0.82 ± 0.17	1				

The search region that contributes the most to the analysis sensitivity in this model is the HH SR31 which requires $E_{\mathrm{T}}^{\mathrm{miss}} > 300$ GeV and is inclusive in the other variables. In the region with a large mass difference between the gluino and the LSP, results are rather stable with respect to LSP mass variations, and gluino masses up to 1.28 TeV are excluded. Near the kinematic limit of $m(\tilde{\mathrm{g}}) - m(\tilde{\chi}^0) = 2 \cdot (m(\mathrm{W}) + m(\mathrm{b}))$, the gluino mass limit becomes weaker and goes down to about 1 TeV for an LSP mass of 800 GeV. These results extend the sensitivity obtained in the previous analysis [3].

We extract model independent limits on $\sigma \cdot \mathcal{A} \cdot \epsilon$ in the two semi-inclusive signal regions in the HH category, SR31 and SR32. In SR31 the limit is computed as a function of the minimum threshold on $E_{\mathrm{T}}^{\mathrm{miss}}$ (for $H_{\mathrm{T}} > 300$ GeV), while in SR32 the limit is computed as function of the H_{T} threshold (for $50 < E_{\mathrm{T}}^{\mathrm{miss}} < 300$ GeV). The limits are computed assuming full efficiency for $E_{\mathrm{T}}^{\mathrm{miss}}$ and H_{T}, while the lepton efficiency ranges between 70–90% (50–75%) for generated muons (electrons) with $|\eta| < 2.4$ and $p_{\mathrm{T}} > 25$ GeV, increasing as a function of p_{T} and reaching the plateau value for $p_{\mathrm{T}} > 60$ GeV. Results are shown in Fig. 5.

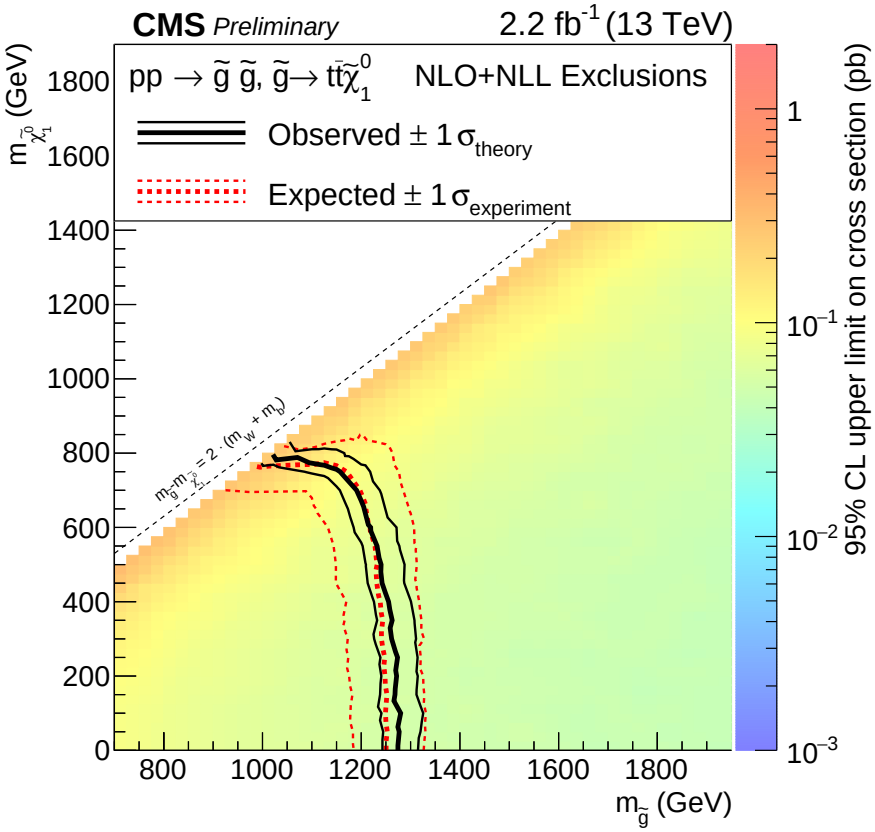

Figure 4: Exclusion regions at a 95% CL in the plane of $m(\tilde{\chi}^0)$ versus $m(\tilde{\mathrm{g}})$ for the T1tttt simplified model. The right-hand-side color scale indicates the excluded cross section values for a given point in the SUSY particle mass plane. Observed and expected limit lines indicate the boundaries of excluded regions (to the left and below the curve).

7 Summary

We have presented the results of a search for BSM physics with same-sign dileptons using the CMS detector at the LHC, based on a 2.2 fb^{-1} data sample of pp collisions at $\sqrt{s} = 13$ TeV. The

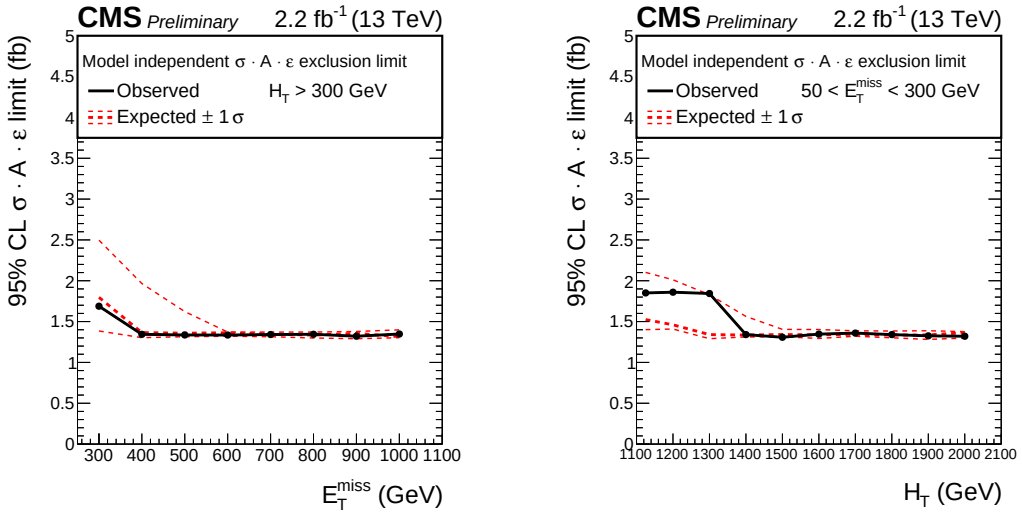

(a) (b)

Figure 5: Limitis on $\sigma \cdot \mathcal{A} \cdot \epsilon$ at 95% CL with $\mathcal{L} = 2.2$ fb^{-1}.

data are analyzed in exclusive signal regions defined with different selections on lepton and event kinematic variables, as well as jet and b jet multiplicities.

No significant deviations from the standard model expectations are observed. The results are used to set upper limits on the gluino pair production in the T1tttt simplified model. Gluino masses are probed up to 1.28 TeV, thus significantly extending the sensitivity of previous dilepton searches.

References

[1] CMS Collaboration, "The CMS experiment at the CERN LHC", *JINST* **3** (2008) S08004, doi:10.1088/1748-0221/3/08/S08004.

[2] CMS Collaboration, "Search for new physics in events with same-sign dileptons and b jets in pp collisions at $\sqrt{s} = 8$ TeV", *JHEP* **03** (2013) 037, doi:10.1007/JHEP03(2013)037, 10.1007/JHEP07(2013)041, arXiv:1212.6194.

[3] CMS Collaboration, "Search for new physics in events with same-sign dileptons and jets in pp collisions at 8 TeV", *JHEP* **01** (2014) 163, doi:10.1007/JHEP01(2014)163, arXiv:1311.6736.

[4] CMS Collaboration, "Performance of CMS muon reconstruction in pp collision events at sqrt(s) = 7 TeV", *JINST* **7** (2012) P10002, doi:10.1088/1748-0221/7/10/P10002, arXiv:1206.4071.

[5] CMS Collaboration, "Performance of Electron Reconstruction and Selection with the CMS Detector in Proton-Proton Collisions at vs = 8 TeV", *JINST* **10** (2015) P06005, doi:10.1088/1748-0221/10/06/P06005, arXiv:1502.02701.

[6] K. Rehermann and B. Tweedie, "Efficient Identification of Boosted Semileptonic Top Quarks at the LHC", *JHEP* **03** (2011) 059, doi:10.1007/JHEP03(2011)059, arXiv:1007.2221.

[7] CMS Collaboration, "Performance of the CMS missing transverse momentum reconstruction in pp data at $\sqrt{s}$ = 8 TeV", *JINST* **10** (2015) P02006, doi:10.1088/1748-0221/10/02/P02006, arXiv:1411.0511.

[8] M. Cacciari, G. P. Salam, and G. Soyez, "The anti-k_T jet clustering algorithm", *JHEP* **04** (2008) 063, doi:10.1088/1126-6708/2008/04/063, arXiv:0802.1189.

[9] CMS Collaboration, "Jet Energy Calibration in the 8 TeV pp data", CMS Physics Analysis Summary CMS-PAS-JME-13-004, 2015.

[10] CMS Collaboration, "Identification of b-quark jets with the CMS experiment", *JINST* **8** (2013) P04013, doi:10.1088/1748-0221/8/04/P04013, arXiv:1211.4462.

[11] CMS Collaboration, "Performance of b tagging at sqrt(s)=8 TeV in multijet, $t\bar{t}$ and boosted topology events", CMS Physics Analysis Summary CMS-PAS-BTV-13-001, 2013.

[12] J. Alwall et al., "The automated computation of tree-level and next-to-leading order differential cross sections, and their matching to parton shower simulations", *JHEP* **07** (2014) 079, doi:10.1007/JHEP07(2014)079, arXiv:1405.0301.

[13] T. Melia, P. Nason, R. Rontsch, and G. Zanderighi, "W+W-, WZ and ZZ production in the POWHEG BOX", *JHEP* **11** (2011) 078, doi:10.1007/JHEP11(2011)078, arXiv:1107.5051.

[14] T. Sjostrand, S. Mrenna, and P. Z. Skands, "A Brief Introduction to PYTHIA 8.1", *Comput. Phys. Commun.* **178** (2008) 852, doi:10.1016/j.cpc.2008.01.036, arXiv:0710.3820.

[15] GEANT4 Collaboration, "GEANT4—a simulation toolkit", *Nucl. Instrum. Meth. A* **506** (2003) 250, doi:10.1016/S0168-9002(03)01368-8.

[16] S. Abdullin et al., "The fast simulation of the CMS detector at LHC", *J. Phys. Conf. Ser.* **331** (2011) 032049, doi:10.1088/1742-6596/331/3/032049.

[17] ATLAS Collaboration, "Search for anomalous production of prompt same-sign lepton pairs and pair-produced doubly charged Higgs bosons with $\sqrt{s} = 8$ TeV pp collisions using the ATLAS detector", *JHEP* **03** (2015) 041, doi:10.1007/JHEP03(2015)041, arXiv:1412.0237.

[18] CMS Collaboration, "Performance of CMS Muon Reconstruction in Cosmic-Ray Events", *JINST* **5** (2010) T03022, doi:10.1088/1748-0221/5/03/T03022, arXiv:0911.4994.

[19] M. V. Garzelli, A. Kardos, C. G. Papadopoulos, and Z. Trocsanyi, "$t\bar{t}W^{\pm}$ and $t\bar{t}Z$ Hadroproduction at NLO accuracy in QCD with Parton Shower and Hadronization effects", *JHEP* **11** (2012) 056, doi:10.1007/JHEP11(2012)056, arXiv:1208.2665.

[20] CMS Collaboration, "Observation of top quark pairs produced in association with a vector boson in pp collisions at $\sqrt{s}$ = 8 TeV", (2015). arXiv:1510.01131. *Submitted to JHEP*.

[21] A. L. Read, "Presentation of search results: The CL_S technique", *J. Phys. G* **28** (2002) 2693, doi:10.1088/0954-3899/28/10/313.

[22] T. Junk, "Confidence level computation for combining searches with small statistics", *Nucl. Instrum. Meth. A* **434** (1999) 435, doi:10.1016/S0168-9002(99)00498-2, arXiv:hep-ex/9902006.

[23] ATLAS and CMS Collaborations, "Procedure for the LHC Higgs boson search combination in summer 2011", ATL-PHYS-PUB-2011-011, CMS NOTE-2011/005, 2011.

[24] W. Beenakker, R. Höpker, M. Spira, and P. M. Zerwas, "Squark and gluino production at hadron colliders", *Nucl. Phys. B* **492** (1997) 51, doi:10.1016/S0550-3213(97)80027-2, arXiv:hep-ph/9610490.

[25] A. Kulesza and L. Motyka, "Threshold resummation for squark-antisquark and gluino-pair production at the LHC", *Phys. Rev. Lett.* **102** (2009) 111802, doi:10.1103/PhysRevLett.102.111802, arXiv:0807.2405.

[26] A. Kulesza and L. Motyka, "Soft gluon resummation for the production of gluino-gluino and squark-antisquark pairs at the LHC", *Phys. Rev. D* **80** (2009) 095004, doi:10.1103/PhysRevD.80.095004, arXiv:0905.4749.

[27] W. Beenakker et al., "Soft-gluon resummation for squark and gluino hadroproduction", *JHEP* **12** (2009) 041, doi:10.1088/1126-6708/2009/12/041, arXiv:0909.4418.

[28] W. Beenakker et al., "Squark and gluino hadroproduction", *Int. J. Mod. Phys. A* **26** (2011) 2637, doi:10.1142/S0217751X11053560, arXiv:1105.1110.

[29] M. Krämer et al., "Supersymmetry production cross sections in pp collisions at $\sqrt{s} = 7$ TeV", (2012). arXiv:1206.2892.

[30] C. Borschensky et al., "Squark and gluino production cross sections in pp collisions at $\sqrt{s}$ = 13, 14, 33 and 100 TeV", *Eur. Phys. J. C* **74** (2014) 3174, doi:10.1140/epjc/s10052-014-3174-y, arXiv:1407.5066.